

**UNCLASSIFIED**

**AD 404 912**

---

**DEFENSE DOCUMENTATION CENTER**

**FOR**

**SCIENTIFIC AND TECHNICAL INFORMATION**

**CAMERON STATION, ALEXANDRIA, VIRGINIA**



**UNCLASSIFIED**

NOTICE: When government or other drawings, specifications or other data are used for any purpose other than in connection with a definitely related government procurement operation, the U. S. Government thereby incurs no responsibility, nor any obligation whatsoever; and the fact that the Government may have formulated, furnished, or in any way supplied the said drawings, specifications, or other data is not to be regarded by implication or otherwise as in any manner licensing the holder or any other person or corporation, or conveying any rights or permission to manufacture, use or sell any patented invention that may in any way be related thereto.

63-3-5

ASD-TDR-62-978

CATALOG BY ASTIA

404912

404 912

## DEVELOPMENT OF A FAST SOLID-STATE ULTRAVIOLET PHOTODETECTOR

TECHNICAL DOCUMENTARY REPORT NO. ASD-TDR-62-978

March 1963

Electronic Technology Laboratory  
Aeronautical Systems Division  
Air Force Systems Command  
Wright-Patterson Air Force Base, Ohio

Project No. 4460, Task No. 446004

(Prepared under Contract No. AF33(616)-8410  
by Institute of Science and Technology,  
The University of Michigan,  
Ann Arbor, Michigan  
Authors: Douglas E. Brown,  
Richard C. Keezer, Joseph Mudar)

DDC  
MAY 29 1963  
JISIA D

## NOTICES

When Government drawings, specifications, or other data are used for any purpose other than in connection with a definitely related Government procurement operation, the United States Government thereby incurs no responsibility nor any obligation whatsoever; and the fact that the Government may have formulated, furnished, or in any way supplied the said drawings, specifications, or other data, is not to be regarded by implication or otherwise as in any manner licensing the holder or any other person or corporation, or conveying any rights or permission to manufacture, use, or sell any patented invention that may in any way be related thereto.

Qualified requesters may obtain copies of this report from the Armed Services Technical Information Agency, (ASTIA), Arlington Hall Station, Arlington 12, Virginia.

This report has been released to the Office of Technical Services, U.S. Department of Commerce, Washington 25, D.C., in stock quantities for sale to the general public.

Copies of this report should not be returned to the Aeronautical Systems Division unless return is required by security considerations, contractual obligations, or notice on a specific document.

## **FOREWORD**

This report was prepared by the Institute of Science and Technology of The University of Michigan, on Air Force Contract AF 33(616)-8410, under Task 446004 of Project 4460 "Development of a Fast Solid-State Ultraviolet Photodetector." The work was administered under the direction of the Electronic Technology Laboratory, Aeronautical Systems Division. Mr. Bryan H. Hill was project engineer for the Laboratory.

The study began in June, 1961, and concluded in August, 1962. Dr. Sol Nudelman, Semiconductor Group Leader, was Principal Investigator on the Project until he terminated in December, 1961. His replacement was Dr. Douglas E. Brown. Chief contributors to the Project were Richard C. Keezer and Joseph Mudar.

This is the final report and concludes the work on Contract AF 33(616)-8410. The contractor's report number is 4611-13-F.

This report is unclassified.

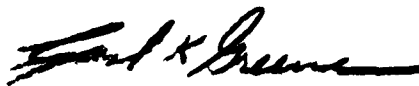
# ABSTRACT

The objective of this work was to develop a fast solid-state ultraviolet detector. Efforts were concentrated on photovoltaic devices using metal semiconductor barrier layers. Peak detectivities of the order of  $10^9$  cm cps<sup>1/2</sup>/watt and time constants of less than 120  $\mu$ sec were achieved with both ZnS ( $\lambda_{\text{peak}} = 339$  m $\mu$ ) and TiO<sub>2</sub> ( $\lambda_{\text{peak}} = 320$  m $\mu$ ). MgO was found to be photoconductive when exposed to radiation of wavelength less than 260 m $\mu$ . Trapping states in TiO<sub>2</sub> were investigated by means of the method of space-charge-limited currents.

## PUBLICATION REVIEW

This technical documentary report has been reviewed and is approved.

FOR THE COMMANDER:



CARL K. GREENE  
Phenomena Exploitation Section  
Molecular Electronics Branch  
Electronic Technology Laboratory

## CONTENTS

1. Introduction . . . . .	1
2. Barrier-Layer Properties . . . . .	2
3. Experimental Program . . . . .	4
3.1. Measurement Procedures	4
3.2. Zinc Sulfide	8
3.3. Rutile ( $\text{TiO}_2$ )	15
3.4. Other Materials	24
4. Summary and Conclusions . . . . .	25
Appendix A: Equivalent-Circuit Analysis . . . . .	26
Appendix B: Space-Charge-Limited Currents . . . . .	31
References . . . . .	33

**FIGURES**

1. Spectral-Response Measuring Equipment . . . . .	5
2. Detector-Evaluating Equipment . . . . .	5
3. Detector-Evaluating Electronics . . . . .	6
4. Cathode-Follower Preamplifier . . . . .	7
5. Time-Constant Measuring Equipment . . . . .	7
6. Zinc Sulfide Current Characteristics . . . . .	9
7. Signal Waveforms of ZnS Detector Showing Dependence of Signal Amplitude and Time Constant on Back Bias Voltage . . . . .	10
8. Signal Waveform of 120 $\mu$ sec Response ZnS Detector — High Chopping Speeds . . . . .	11
9. Signal Waveform of 120 $\mu$ sec Response ZnS Detector — Low Chopping Speeds . . . . .	11
10. Signal Waveforms of a ZnS Detector Showing Effect of Bias Voltage on Signal Amplitude and Time Constant . . . . .	12
11. Spectral Response—Zinc Sulfide Detector . . . . .	13
12. Transmission of Rutile and Silver Film . . . . .	15
13. Rectification Properties (Rutile) . . . . .	17
14. Spectral Response—Rutile Detectors . . . . .	17
15. Photovoltaic Decay (Multi-Time-Constant Detector) . . . . .	18
16. Cross Section of Reduced-Reoxidized Rutile Detector . . . . .	20
17. Detectivity of Rutile Detectors . . . . .	20
18. Effect of Trap States on Reduced Current (Rutile) . . . . .	24
19. Response of Equivalent Circuit to Step Input . . . . .	30

**TABLE**

I. Effect of Reoxidation on Time Constant of Rutile Detectors . . . . .	22
---	----

## DEVELOPMENT OF A FAST SOLID-STATE ULTRAVIOLET PHOTODETECTOR\*

### 1 INTRODUCTION

The objective of this program was to develop a fast solid-state ultraviolet detector. Materials suitable for the fabrication of such devices are semiconductors with large (3.5 ev and greater) forbidden bandgaps. These semiconductors are often characterized by high resistivity, low carrier mobility, and long excess carrier lifetime. As described in the following report, these characteristics constituted the principal sources of difficulty in developing an ultraviolet detector.

Zinc sulfide and rutile were two semiconducting materials selected for primary investigation early in the program. Zinc sulfide was known to have photoresponse in the ultraviolet at wavelengths out to 350 m $\mu$ . It has also been used successfully in a light amplifier utilizing the mechanism of carrier multiplication [1]. High-purity single crystals are available, and much information concerning the material is in the literature. Early experiments on ZnS crystals on hand indicated a bulk resistivity of  $7.6 \times 10^9$  ohm-cm. The resistivity was significantly reduced by exposure to ultraviolet radiation.

Excellent barrier-layer rectifiers have been made with rutile (TiO<sub>2</sub>) [2]. This material has a forbidden bandgap of 3.67 ev, which would lead to a cutoff wavelength of 338 m $\mu$ . It is available in large single crystals. In preliminary experiments using deposited films of rutile, reduction followed by reoxidation was found to enhance the ultraviolet photoresponse. The mode of operation was photoconductive.

---

\*Manuscript released by the author, August 1962, for publication as an ASD Technical Documentary Report.

Consideration was given to the most desirable method of ultraviolet detection. The basic mechanisms involved in photoconductive, photovoltaic, and photoelectromagnetic operation were reexamined. As a result of this study, it was decided to concentrate efforts on the photovoltaic mode of operation. This decision was based primarily on two facts: (1) the mobility of charge carriers is low in most near-insulating semiconductors; and (2) the absorptivity of the materials for ultraviolet radiation is high. These two facts indicate the desirability of a detector with a thin, layer-type, sensitive volume. Such a device is obtainable through use of barrier-layer techniques, which lend themselves to photovoltaic operation.

## 2

### BARRIER-LAYER PROPERTIES

Placing a metal in contact with a semiconductor often modifies the semiconductor charge distribution near the contact boundary. Thus, an n-type semiconductor in contact with a metal of larger work function loses electrons to the metal. At equilibrium, with the Fermi levels at the same value throughout both materials, there will be a layer of negative charge on the metal; and a positively charged, high-resistivity, electron-depletion region in the semiconductor near the contact. The potential barrier formed by the charge rearrangement results in a rectifying junction or "barrier layer" [3].

When a voltage  $V$  is applied to such a barrier layer, the voltage-current relation (assuming that the voltage is dropped across the barrier) is given by

$$J = J_g [\exp(eV/kT) - 1] \quad (1)$$

where  $J$  = total current density

$J_g$  = saturation current density

$k$  = Boltzmann constant

$T$  = absolute temperature

$e$  = electronic charge

This relation is of the same form as that for a p-n junction. The value of  $J_g$  is difficult to predict for barrier-layer rectifiers.

A barrier layer will have a capacitance since it consists of two regions of relatively high conductivity separated by the low-conductivity depletion region. The capacity per unit area is proportional to the dielectric constant of the depletion layer and inversely proportional to the width of the depletion region. The application of a potential across the barrier layer changes this width according to the relation [4].

$$X^2 = \frac{\epsilon(\phi - U + V)}{2\pi n e} \quad V \geq -(\phi + U) \quad (2)$$

where  $X$  = the barrier-layer width

$V$  = applied voltage—considered positive in the reverse bias direction

$\epsilon$  = dielectric constant

$\phi$  = difference in work functions between metal and semiconductor

$U$  = Fermi level of semiconductor, measured from conduction band

$n$  = free-carrier density

In thermal equilibrium the excess positive and negative charge layers are maintained by the potential barrier established. When ionizing radiation is absorbed in the vicinity of the barrier, the extra free charge carriers thus generated diffuse to the junction and result in a rearrangement of the charge distribution.

This reduces the potential barrier, and under appropriate conditions the change in barrier potential can be detected as a light-induced voltage. This is known as the photovoltaic effect. For the open circuit (no net current) condition the small signal photovoltage is given by [3]

$$V = \frac{kT}{e} \ln(1 + KG) \quad (3)$$

where  $K$  = a material constant

$G$  = volume generation rate of electron hole pairs

The photovoltage is proportional to the generation rate only for small values of  $G$ . At sufficiently high values of  $G$  the potential barrier, and thus any further photovoltaic effect, is eliminated. Hence the magnitude of the potential barrier is the limiting value of the photovoltage attainable.

The time constant associated with the photovoltaic effect is approximately equal to the excess carrier lifetime. In material containing traps, the effective excess carrier lifetime may be increased. If one assumes that the small signal response of the detector is proportional to the concentration of excess carriers, it is easy to show that the decay of response on interrupting the ionizing radiation is

$$V = c \exp(-t/\tau) \quad (4)$$

where  $V$  = signal voltage

$c$  is a constant

$t$  = time measured from termination of illumination

$\tau$  = effective time constant

The time constant of an actual barrier-layer detector made of near-insulating materials may be determined by the bulk resistance, and distributed capacitance, of the detector. These effects are analyzed in detail in Appendix A.

In evaluating detector performance, one must consider electrical noise properties in addition to responsivity and time constants. Several sources of electrical noise are involved in the consideration of barrier-layer detectors made of high resistivity semiconductors. Johnson, or thermal-agitation, noise may be appreciable. If the active barrier layer occupies a small fraction of the total semiconductor volume, much of the Johnson noise is contributed by essentially inactive material electrically, in series with the barrier layer. For this reason, and also for the purpose of reducing RC time constants, it is desirable that the inactive volume of semiconductor material be minimized.

Statistical fluctuations in the dynamic balance of charge carriers in the vicinity of the barrier layer contribute electrical noise, as does the random release of carriers from trap states within the barrier region. Similarly, statistical fluctuation in generation-recombination processes involving thermal and photon excitation of carriers also act as sources of noise.

Photovoltaic operation involves little net current flow; hence current noise is not especially significant. When biased operation was investigated, an increase in noise level, presumably from current noise, was noticed.

### 3

## EXPERIMENTAL PROGRAM

### 3.1. MEASUREMENT PROCEDURES

The equipment used for measuring the relative spectral response of the detectors is diagrammed in Figure 1. It consisted of a source of ultraviolet radiation, a chopper to interrupt the radiation, a monochromator, an electronic amplifier, a wave analyzer to measure the signal output in a narrow-frequency band centered at the chopping frequency, and a cathode ray oscilloscope to observe the wave form (Figures 2 and 3).

The ultraviolet source was a Bausch and Lomb d-c hydrogen arc lamp. Radiation from the lamp was chopped at 20 cps, collected by a mirror, and focused onto the entrance of a Bausch

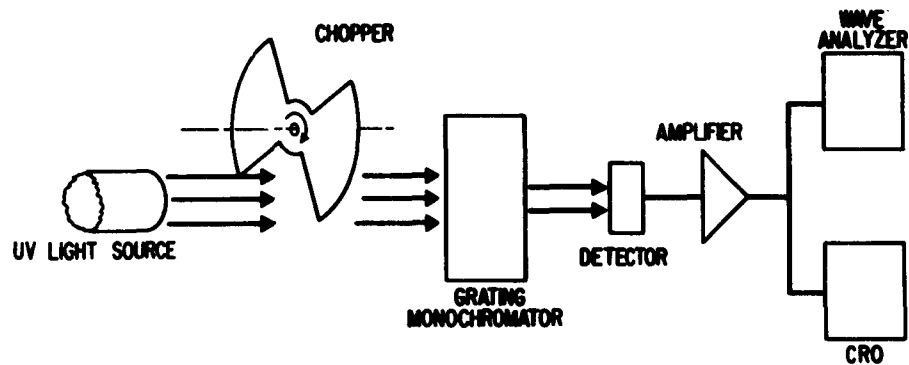


FIGURE 1. SPECTRAL-RESPONSE MEASURING EQUIPMENT



FIGURE 2. DETECTOR-EVALUATING EQUIPMENT

and Lomb grating monochromator. The monochromator used 250-mm focal-length optics and a 600 line/mm grating, producing an average linear dispersion of  $6.6 \text{ m}\mu/\text{mm}$  at the exit slit. Exit and entrance slit widths varied according to the sensitivity of the detector used and the spectral region being observed.



FIGURE 3. DETECTOR-EVALUATING  
ELECTRONICS

A cathode follower was used to match the impedance of the detector to that of the preamplifier (Figure 4). A general radio-wave analyzer having a 5-cps bandwidth was used to measure the amplified signal and noise.

The procedure for determining the absolute detectivity of the detectors was similar to that followed in making spectral response measurements. The monochromator was set at a given wavelength and the detector signal-to-noise ratio determined for a given radiant flux density. The monochromatic radiant flux density was determined with a Reeder thermocouple. The thermocouple in turn was calibrated with a Barnes blackbody. From these data and a knowledge of the sensitive area of the detector, the  $D^*_\lambda$  value for the detector is given by

$$D^*_\lambda = \frac{\sqrt{A\Delta f}}{NEP_\lambda} \text{ cm cps}^{1/2}/\text{watt} \quad (5)$$

where  $A$  = sensitive area of detector

$\Delta f$  = electrical bandwidth of measuring effort

$NEP_\lambda$  = measured noise equivalent power at wavelength  $\lambda$

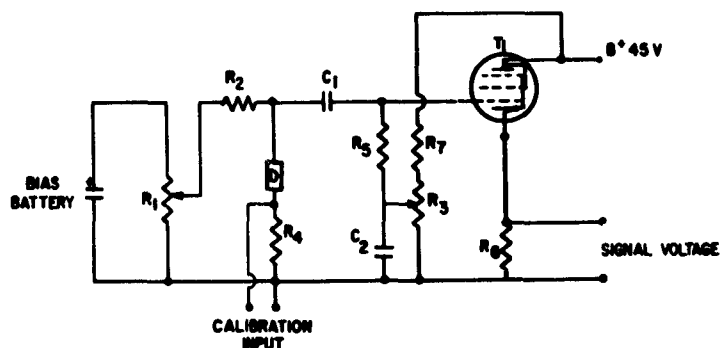


FIGURE 4. CATHODE-FOLLOWER PREAMPLIFIER

D = detector $10 \text{ meg } \Omega$	$R_6 = 200\text{K wire wound}$
$R_1 = 50\text{K helipot}$	$R_7 = 120\text{K wire wound}$
$R_2 = 200 \text{ meg } \Omega$	$C_1 = 0.022 \mu\text{fd @ 400 volts}$
$R_3 = 50\text{K helipot}$	$C_2 = 10 \mu\text{fd @ 25 volts}$
$R_4 = 5\Omega \text{ test resistor}$	$T_1 = \text{RCA} - 6\text{CB6}$
$R_5 = 400 \text{ meg } \Omega$	

The equipment for measuring time constants is diagramed in Figure 5. The hydrogen arc lamp is again used as a source. The radiation is collected by a mirror and focused in the plane of a variable-speed chopper. After passing through the chopper the radiation is incident on the detector. The response of the detector to the radiation is then electronically amplified and displayed on an oscilloscope. The time constant is defined as the time required for the response to rise to  $1 - 1/e$  of its maximum response. The equipment has a capability of measuring time constants down to  $20 \mu\text{sec}$ .

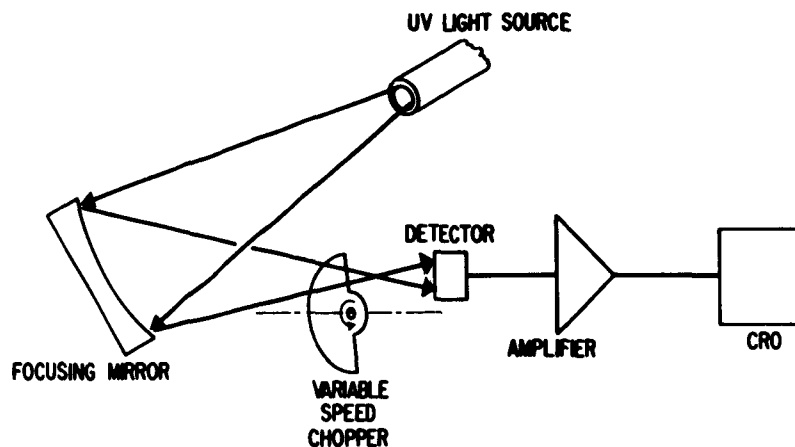


FIGURE 5. TIME-CONSTANT MEASURING EQUIPMENT

### 3.2. ZINC SULFIDE

At room temperature crystalline ZnS can exist in two forms, cubic and hexagonal. Pure cubic ZnS is colorless, has an index of refraction of 2.37, a specific gravity of 4.102, and a lattice constant of 5.41 Å. Cubic ZnS makes a transition to a hexagonal crystal structure at temperatures above 1030°C.

Hexagonal ZnS is colorless, has an index of refraction of 2.36, a specific gravity of 4.087, and lattice constants of  $a = 3.811$  Å,  $c = 6.234$  Å. The melting point is 1850°C. However, it sublimes at 1185°C, thus permitting crystal growth at temperatures lower than the melting point.

**3.2.1. DETECTOR PREPARATION.** Single crystals of ZnS were grown by a sublimation process. Luminescent grade ZnS power was vaporized in a glass bomb heated to 1450°C and allowed to recrystallize on a cooled portion of the bomb. Although the boules thus formed were polycrystalline, large single-crystal portions could be selected. The type or concentration of carriers in the resulting single crystals was not determined directly, but subsequent measurements on the finished detectors indicated an "n" type of conductivity.

This procedure was used to fabricate detectors from these boules.

- (a) Slices approximately 1 mm thick were cut from the boule with a diamond saw.
- (b) By means of a series of successively finer grits the slice was ground and polished down to a thickness of about 500μ. The final polish was on an optically flat lap using a Linde 0.3A polishing compound.
- (c) An indium electrode was evaporated onto one side of the polished slice and bonded to a glass disc by means of a conducting epoxy.
- (d) The crystal was polished until the thickness was less than 25μ and again finished with a final lap on an optical flat.
- (e) A transparent electrode of Cu or Ag was evaporated on the front surface. Finally, fine Cu wire leads were cemented to the electrodes with silver paste.

**3.2.2. GENERAL DETECTOR CHARACTERISTICS.** Since indium is reported to produce ohmic contacts with ZnS [5], and Cu or Ag produce non-ohmic or rectifying contacts, the detector voltage-current characteristics were expected to be those of a barrier-layer rectifier (i.e., follow a relationship given by Equation 1). Initially, the first detector fabricated did show a rectifying property,  $I_{\text{forward}}/I_{\text{reverse}} = 20$ . This property deteriorated over a period of two weeks until essentially all rectification had disappeared. The current then exhibited an exponential dependence on applied voltage over the measured voltage range for both positive and

negative values of the voltage (Figure 6). This type of behavior is similar to that observed with space-charge-limited currents (see Appendix B).

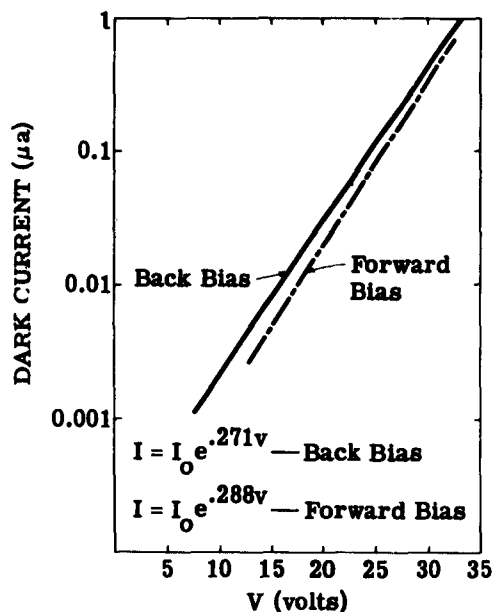


FIGURE 6. ZINC SULFIDE CURRENT CHARACTERISTICS

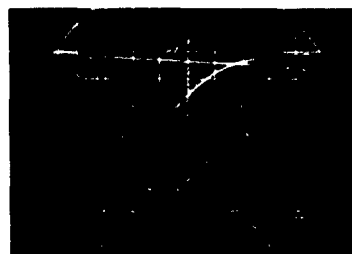
This unit, ZnS-1, approximately  $25\mu$  thick, exhibited both photovoltaic and photoconductive response to ultraviolet radiation. The time constant was approximately 25 msec. Since the time constant of semiconducting detectors is a function of the trap population and depth, two methods of depopulating traps and thus decreasing the time constant were tried on this detector: (1) increasing the bias voltage across the detector; (2) illuminating the detector with intense unvarying radiation from an incandescent lamp. No variation of time constant was observed. This suggested that distributed capacitance and the high impedance associated with this type of detector could be the important parameters in determining the time constant. An equivalent circuit was assumed and the response of the circuit to a square voltage pulse was analyzed (see Appendix A). The value for the time constant calculated from the results of this analysis (50 msec) compared well with the observed value. This indicated that the resistance and capacitance inherent in this detector could very well limit the minimum observable time constant.

To decrease the resistance, we made subsequent detectors from lower resistivity materials polished them to thicknesses of less than  $25\mu$ . The detectors, ZnS-2, 3, 4, fabricated from the second, lower-resistivity boule had photovoltaic characteristics similar to ZnS-1. They were approximately  $15\mu$  thick. In the photoconductive mode of operation, they exhibited marked dependence of the time constant on bias voltage. Operating with zero bias voltage (photovoltaic),

the detectors had time constants of approximately 2.5 msec. However, as the bias voltage increased in the reverse direction (i.e., front Cu electrode minus) the time constant also increased, reaching a value of about 150 msec at 10.5 volts bias (Figure 7).



(a) bias = 0 volts  
sensitivity = 5 mv/large division  
sweep speed = 5 msec/large division



(b) bias = 10 1/2 volts  
sensitivity = 500 mv/large division  
sweep speed = 100 msec/large division

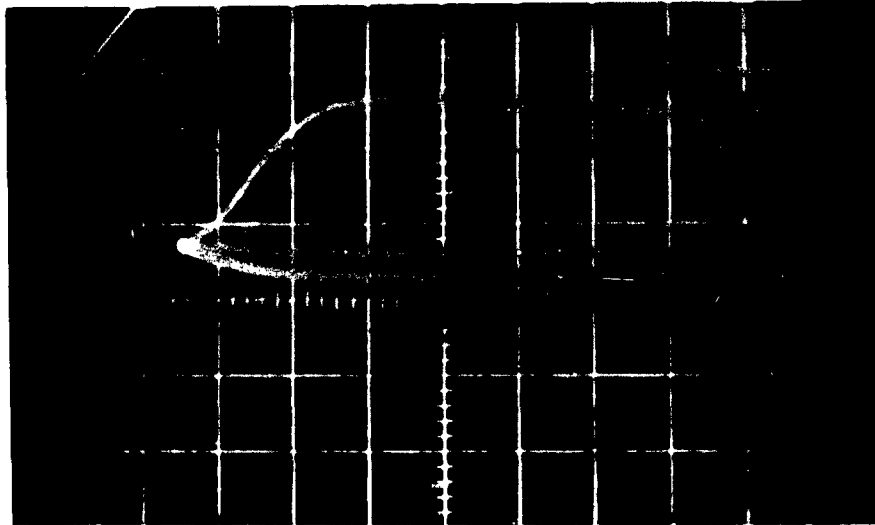
FIGURE 7. SIGNAL WAVEFORMS OF ZnS DETECTOR SHOWING DEPENDENCE OF SIGNAL AMPLITUDE AND TIME CONSTANT ON BACK BIAS VOLTAGE

ZnS-5, the fastest ZnS detector fabricated to date, was polished to a thickness such that white light fringes were visible. This detector had a time constant of approximately 120  $\mu$ sec (Figure 8). It had properties markedly different from those of the other detectors. The response to low-frequency chopped radiation is shown in Figure 9. This type of response, the sharp rise followed by a relatively slow decay to a finite d-c value, was not observed in the other ZnS detectors. It is consistent with the results predicted on the basis of the equivalent circuit (Appendix A), if it is assumed that the extreme thinness of the unit results in a small-series bulk-resistance,  $R_b$ , and a large bulk capacity,  $C_b$ .

Another peculiarity of this detector is the insensitivity of the response to bias current. The signal amplitude and time constant remained constant with increasing bias current; however, random noise greatly increased.

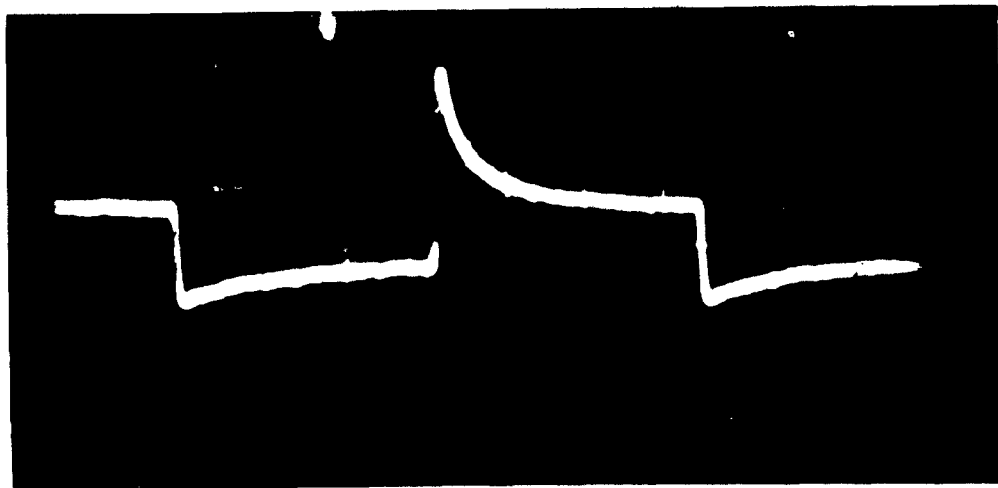
All of the detectors demonstrated photovoltaic and photoconductive response. In the photoconductive mode the signal appeared to be a composite of two independent modes of signal generation. With reverse bias, (Cu electrode -, Indium electrode +), the signals from the photovoltaic and photoconductive modes add, and the signal amplitude increases with increasing bias voltage. However, with forward bias ( $\text{Cu}^+$ ,  $\text{In}^-$ ) the two signals subtract until the photoconductive signal predominates. Figure 10 shows this as the bias is increased from zero to one volt.

Although the ZnS bulk detectors have followed the trend that reducing the thickness results in a reduction in time constant, a quantitative relationship between thickness and time constant has not been determined.



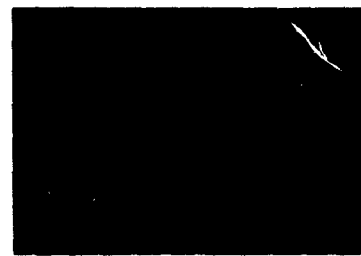
$\tau = 120 \mu\text{sec}$   
 sensitivity = 1 mv/large division  
 sweep speed = 100  $\mu\text{sec}$ /large division

FIGURE 8. SIGNAL WAVEFORM OF 120  $\mu\text{sec}$  RESPONSE ZnS DETECTOR—HIGH CHOPPING SPEEDS



$\tau = 120 \mu\text{sec}$   
 sensitivity = 1 mv/large division  
 sweep speed = 1 msec/large division

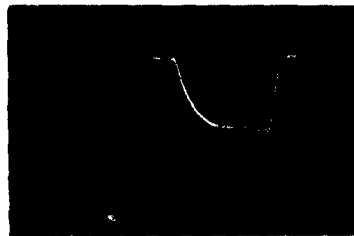
FIGURE 9. SIGNAL WAVEFORM OF 120  $\mu\text{sec}$  RESPONSE ZnS DETECTOR—LOW CHOPPING SPEEDS



(a)  $t_0 \rightarrow$  bias = 0 volts



(d)  $t_0 \rightarrow$  bias = 450 mv



(b)  $t_0 \rightarrow$  bias = 150 mv



(e)  $t_0 \rightarrow$  bias = 600 mv



(c)  $t_0 \rightarrow$  bias = 300 mv



(f)  $t_0 \rightarrow$  bias = 1 volt

sensitivity = 1 mv/large division  
sweep speed = 5 msec/large division

FIGURE 10. SIGNAL WAVEFORMS OF A ZnS DETECTOR SHOWING EFFECT OF BIAS VOLTAGE ON SIGNAL AMPLITUDE AND TIME CONSTANT

Exposure of the ZnS bulk detectors to a vacuum for a period of 24 hours had no measurable effect on the time constant or other characteristics.

**3.2.3. RELATIVE SPECTRAL RESPONSE.** The spectral response of the ZnS detectors did not vary appreciably from detector to detector, or with mode of operation. A spectral response curve representative of these detectors is shown in Figure 11. They exhibit a sharp response peak at  $339\text{ m}\mu$ , falling off rapidly with increasing wavelengths. The response is down to 5% of peak at approximately  $350\text{ m}\mu$ .

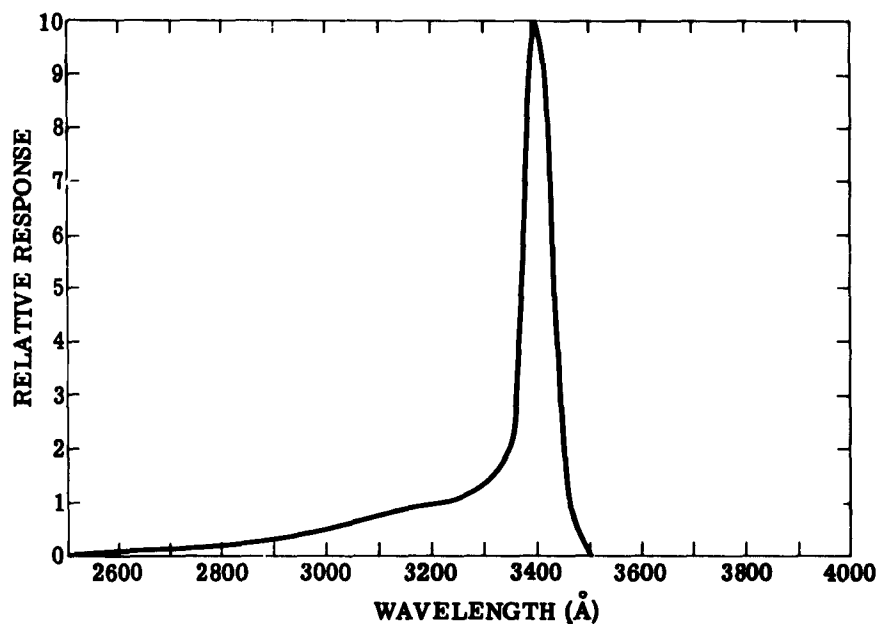


FIGURE 11. SPECTRAL RESPONSE—ZINC SULFIDE DETECTOR

The response on the short-wavelength side of the peak deviates from the "saw-tooth" usually associated with quantum detectors, in that the response falls off very rapidly to about  $330\text{ m}\mu$ , then decreases gradually out to about  $250\text{ m}\mu$ . Moss explains this deviation from a saw-tooth response on the basis of differences in the bulk and surface recombination velocities [6].

**3.2.4. ABSOLUTE RESPONSE (ZnS-5).** Using  $f/4$  optics to collect and focus radiation from the hydrogen arc lamp onto the detector, we observed photovoltaic signals in the millivolts. Johnson noise associated with these high impedance detectors sets the limit on the absolute detectivity. The measured rms detector noise was of the order of  $10\text{ }\mu\text{v}$  in a 5-cps bandwidth.

This compares with  $7 \mu\text{v}$  calculated for a detector having a d-c resistance of  $10^9 \Omega$ . The absolute detectivity for ZnS-5 was measured at the wavelength at which the detector spectral response curve peaked. The detectivity ( $D_{pk}^*$ ) was  $9.7 \times 10^8 \text{ cm cps}^{1/2}/\text{watt}$  at a chopping frequency of 20 cps and a wavelength of  $339 \text{ m}\mu$ .

**3.2.5. BARRIER-LAYER CAPACITY MODULATION.** Consideration was given to the possibility of detecting ultraviolet radiation by its effect on the capacitance of a barrier layer. For this type of detection to be successful, the following conditions must be fulfilled:

- (a) The capacity of the detector is due primarily to the barrier layer inherent in a rectifying metal-semiconductor contact.
- (b) The thickness of the barrier layer, and hence its capacity, is a function of the biasing voltage and the impinging radiation.
- (c) The capacitance shift due to the impinging radiation is large enough to be observable.

To determine whether these conditions were fulfilled, we constructed an oscillator in which a ZnS-metal barrier layer furnished the capacitance for the LC resonant circuit. The output of the oscillator was fed into a radio receiver having a beat frequency oscillator. After tuning the BFO to the oscillator signal, we detected small changes in the output frequency of the oscillator as a change in the beat frequency. The capability of the equipment was estimated as follows:

$$\text{Resonant frequency} = f_0 = \frac{1}{2\pi \sqrt{L_0 C_0}} \quad (6)$$

$$df_0 = -\frac{1}{4\pi} \frac{L}{(L_0 C_0)^{3/2}} dC_0 = -\frac{1}{2} \frac{f_0 dC_0}{C_0} \quad (7)$$

or

$$\frac{dC_0}{C_0} = -\frac{2df_0}{f_0} \quad (8)$$

The resonant frequency  $f_0$  of the oscillator was  $6.5 \times 10^6 \text{ cps}$ , and it was determined that a shift in resonant frequency of less than 6.5 cps could be identified. Thus, a change in barrier-layer capacity of less than two parts per million should have been detectable. A resonant frequency change as a function of bias voltage could be detected, but no frequency change as a function of ultraviolet radiation intensity was observed. Although large photo-capacitive effects (factors of 2 or 3) have been observed with ZnS powders, Eube indicates that these effects are peculiar to powders and any small change in single crystals can be explained by a change in photoconductivity [5].

### 3.3. RUTILE (TiO<sub>2</sub>)

Single-crystal rutile is produced synthetically by the flame fusion process. It is in the tetragonal crystal system with lattice constants  $a = 4.59 \text{ \AA}$  and  $c = 2.96 \text{ \AA}$ . It belongs to the  $D_{4h}^{14}$  space group and exhibits double refraction. It has a specific gravity of 4.26 and a hardness on the Mohs' scale of 6.5 - 7. The melting point is  $1825^\circ\text{C}$ . The properties of rutile are discussed by Grant [7].

Silica (SiO<sub>2</sub>) and alumina (Al<sub>2</sub>O<sub>3</sub>) are present as major impurities in synthetically produced crystals.

The transmission of single-crystal rutile is shown in Figure 12.

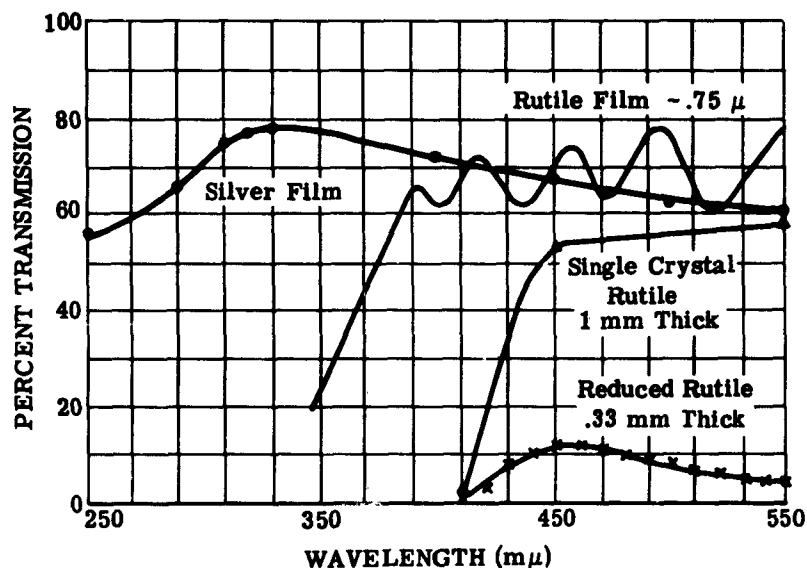


FIGURE 12. TRANSMISSION OF RUTILE AND SILVER FILM

**3.3.1. THIN FILMS.** Thin films of rutile were prepared by spraying a mixture of titanium tetrachloride and a dry carrier gas such as helium onto glass heated to  $150\text{--}300^\circ\text{C}$ . Water vapor in the air reacts with the titanium tetrachloride as follows:



These films of TiO<sub>2</sub> are transparent and appear colored in room illumination because of interference effects. They have been prepared with uniform thickness over an area of several square inches. Figure 12 shows a typical transmission curve.

The film thickness,  $d$ , may be estimated from the wavelengths at the peaks of the transmission interference fringes,  $\lambda_2$  and  $\lambda_1$ , and from the index of refraction  $\mu$  as shown in Equation 10.

$$d = \frac{\Delta n}{2\mu} \left( \frac{\lambda_1 \lambda_2}{\lambda_1 - \lambda_2} \right) \quad (10)$$

where  $\Delta n$  is the number of fringes between  $\lambda_2$  and  $\lambda_1$ . The films may be applied up to several microns thick.

The thin films produced according to the reaction described by Equation 9 had very high resistivities, and initially showed no ultraviolet photoresponse. If the samples were treated by reduction followed by reoxidation, they exhibited photoconductivity when exposed to ultraviolet light. However, since single-crystal rutile (see following sections) showed greater promise of developing into acceptable ultraviolet detectors, work on rutile films was suspended.

**3.3.2. SINGLE-CRYSTAL (NON-REDUCED) DETECTORS.** Cronmeyer reported photoconductivity in unreduced single-crystal rutile in 1952 [8]. Single-crystal material was obtained from the Linde Corporation and from National Lead. Discs 1 mm thick and 3/8" in diameter were cut and polished by techniques similar to those described in Section 3.2. Electrodes were applied to the opposite faces of the discs by evaporation, air drying pastes, or thermally decomposing gold and platinum compounds. The following configurations were investigated.

<u>Top Electrode</u>	<u>Bulk</u>	<u>Bottom Electrode</u>
In	TiO <sub>2</sub>	In
In	TiO <sub>2</sub>	Ag
Ag	TiO <sub>2</sub>	Ag
Au	TiO <sub>2</sub>	Ag
Pt	TiO <sub>2</sub>	Ag
Ag	TiO <sub>2</sub>	In

The top electrode did not cover the entire surface and was opaque. The bottom electrode covered the entire surface and was also opaque. The top surface was exposed to radiation which may be transmitted through the unmasked surface into the bulk.

All configurations except In-TiO<sub>2</sub>-In and Ag-TiO<sub>2</sub>-Ag resulted in photovoltaic response, and exhibited current rectification (Figure 13). Back-to-front resistance ratios as high as 1800:1 were obtained with the Ag-TiO<sub>2</sub>-In configuration. These results indicated formation of a metal-semiconductor barrier layer. Figure 14 shows the relative spectral response for a Ag-TiO<sub>2</sub>-In detector.

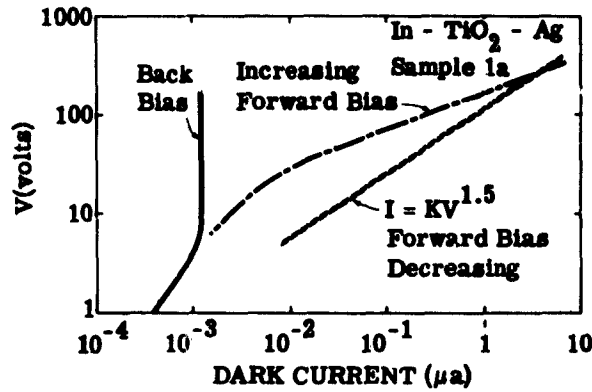


FIGURE 13. RECTIFICATION PROPERTIES  
(RUTILE)

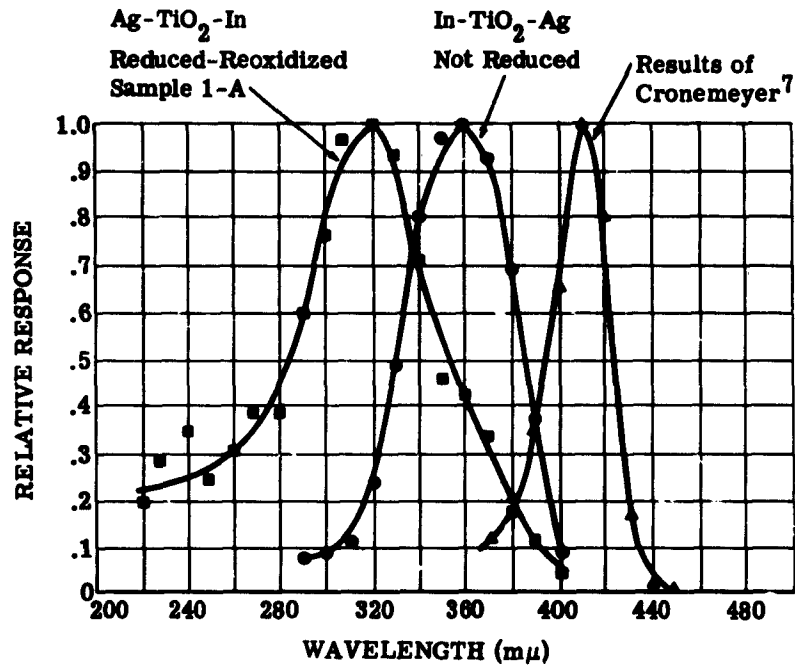


FIGURE 14. SPECTRAL RESPONSE—RUTILE DETECTORS

Time-constant measurements of these detectors were made by the experimental arrangement of Figure 5. The oscilloscope trace of the rise and decay curves was photographed and analyzed. According to Equation 4, a plot of  $\ln(\text{response})$  vs. time should be a straight line with slope  $-1/\tau$ . Figure 15 shows such a plot for a typical detector. It is evident that multiple time constants are found with detectors made from samples of rutile. Time constants of several

hundred milliseconds are common. Thin samples have smaller time constants than thick samples. These results are consistent with the equivalent circuit analysis presented in Appendix A, which indicates that the long time constants can be associated with the high resistance and distributed capacitance of the bulk material. Attempts were then made to reduce the resistance of the bulk material by chemical reduction.

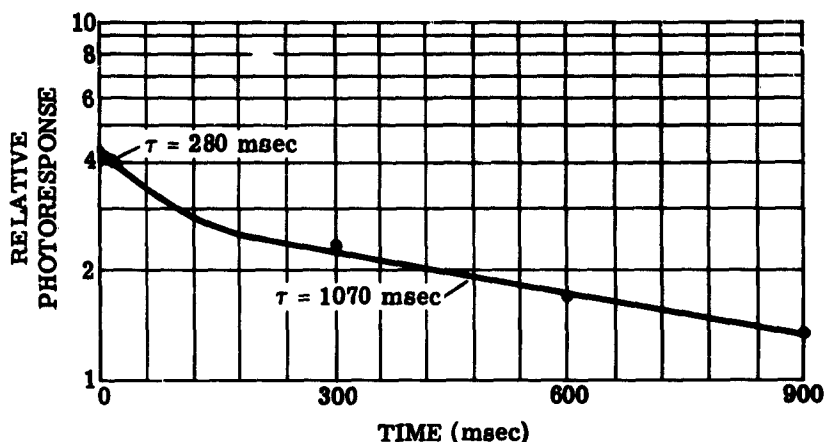
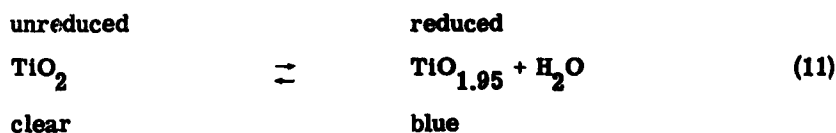
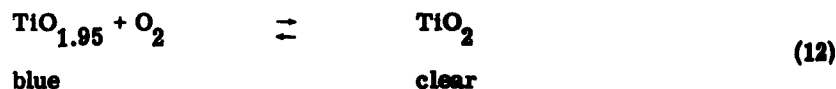


FIGURE 15. PHOTOVOLTAIC DECAY (MULTI-TIME-CONSTANT DETECTOR)

**3.3.3. REDUCTION AND REOXIDATION OF RUTILE.** Non-stoichiometric rutile can be produced by exposing the material to reducing environments [9]. The resulting material has a deficiency of oxygen atoms, which causes a change in appearance from a transparent, slightly yellowish material to an almost opaque blue.



The reaction is quite reversible; however, reoxidation is usually obtained by heating the reduced material in an oxygen atmosphere.



The unreduced material is essentially an insulator, whereas the resistivity of the reduced material may be as low as several ohm-cm.

**3.3.4. PARTIALLY REDUCED DETECTORS.** Discs of rutile were polished and partially reduced for various periods of time in an atmosphere of hydrogen gas, at 600°C. Appropriate electrodes were evaporated onto the front and back surfaces. The photovoltaic responsivity of these detectors was less than that of detectors made from unreduced material; however, the time constant was also shorter. The responsivity decay plots indicated the disappearance of multiple time constants.

The fastest detectors made by this technique had time constants of 3 to 20 msec.

**3.3.5. STRONGLY REDUCED AND REOXIDIZED DETECTORS.** Discs of rutile were reduced for six to eight hours in hydrogen gas at 600°C. (The transmission of a typical sample is shown in Figure 12.) After reduction they were heated for several minutes in air and formed a thin oxide layer on the surface. Indium and partially transparent silver were then evaporated onto the samples. Several of the resulting detectors were found to have time constants less than 100  $\mu$ sec and sufficient responsivity to be suitable as detectors. The resistances of these units are in the order of 10 ohms. Figure 16 shows the physical nature of these detectors. On some samples the bottom oxide layer was polished off before application of the indium electrode. No apparent change in performance was observed.

Figure 17 shows  $D^*$  versus wavelength for several of these detectors.  $D^*$  peak values considerable in excess of  $10^9$  cm-cps<sup>1/2</sup>-watt<sup>-1</sup> are observed. The noise level was within a factor of 10 of Johnson noise. Although the spectral response of most of the TiO<sub>2</sub> detectors peaked at 320 m $\mu$ , some exhibited response maxima at approximately 360 m $\mu$  (see Figure 14). This effect is currently thought to be due to variation in the crystal structure or impurity content of the rutile boule.

**3.3.6. SURFACE EFFECTS.** A rutile detector was prepared by reduction-reoxidation. After one week of exposure to laboratory atmosphere the response and time constant were determined. The detector was placed in a dewar which was then evacuated. After several hours in the vacuum the detector time constant was found to have dropped from 1 msec to 300  $\mu$ s. The responsivity was reduced by a factor of two.

The sample was maintained in a vacuum at  $10^{-5}$  mm of mercury for 50 hours and no further change in the response or time constant was observed.

The sample was then exposed to air at 1 atmosphere. The responsivity immediately doubled, and the time constant returned to 1 msec.

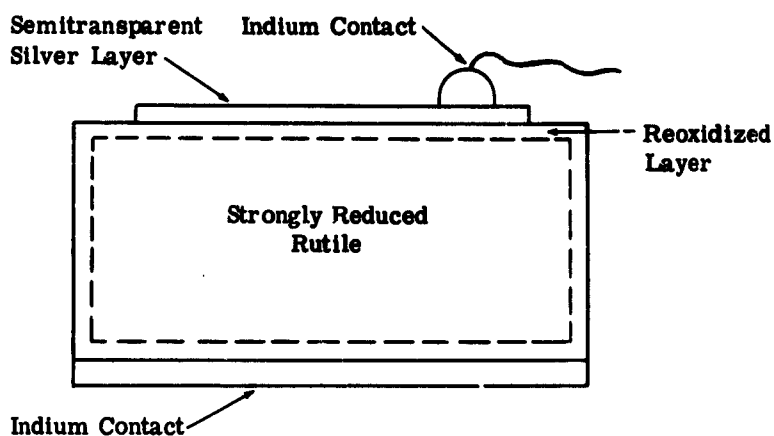


FIGURE 16. CROSS SECTION OF REDUCED-REOXIDIZED RUTILE DETECTOR

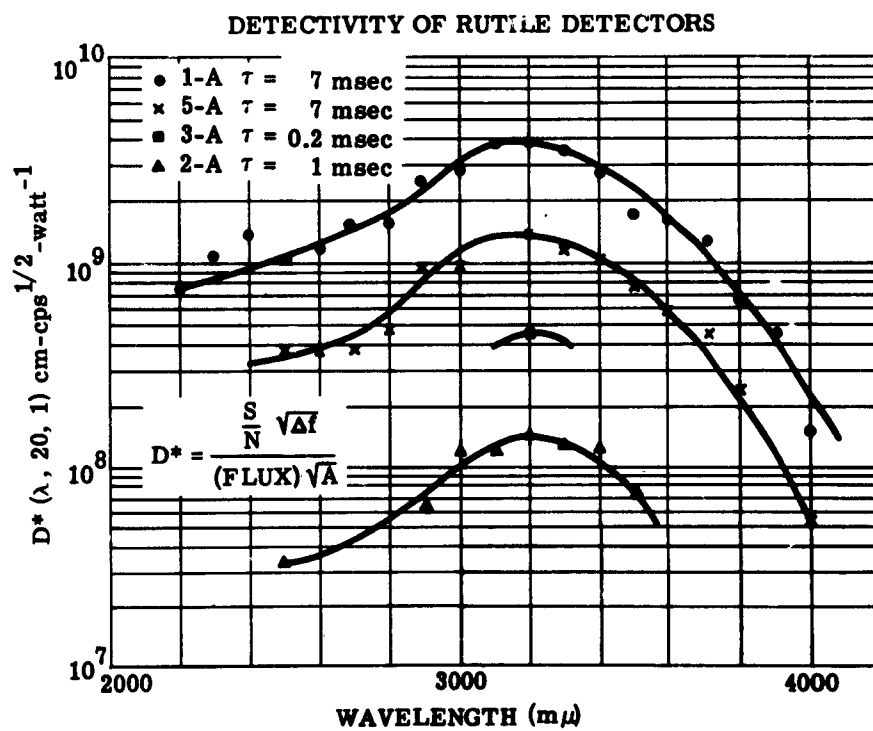


FIGURE 17. DETECTIVITY OF RUTILE DETECTORS

The above experiment was repeated several times, and in each case the responsivity and time constant decreased in vacuum and increased in air.

Although it is presumed that the absorption onto the surface of an atmospheric constituent is responsible for the change in properties, at this time the constituent(s) and its effect are not known.

**3.3.7. EFFECTS OF TEMPERATURE.** One rutile detector was mounted in a dewar, which was evacuated and cooled to liquid nitrogen temperature ( $\sim 100^{\circ}\text{K}$ ). The responsivity increased by about a factor of ten. The time constant also increased. Cronmeyer reported a shift in the photo-response to shorter wavelengths as the temperature is lowered [8].

**3.3.8. THE REDUCED-REOXIDIZED RUTILE PHOTOVOLTAIC DETECTOR.** Detectors made by the reduction-reoxidation technique just described have time constants several orders of magnitude less than those made from single-crystal material as received. It is desirable, therefore, that the performance of these detectors be explained in terms of the reduction-reoxidation procedure.

The experiments performed in an attempt to understand these detectors were as follows.

(a) Four samples were reduced at the same temperature for the same length of time. Two samples were reoxidized. Indium and silver electrodes were evaporated on all four samples. The two samples which had not been reoxidized were not photovoltaic, whereas the reoxidized samples were photovoltaic. This indicated that an oxidized layer is necessary and that fully reduced samples are not photosensitive.

(b) Four samples were reduced and reoxidized together. Indium was evaporated on the back of all four samples and on the front of two samples. Silver was evaporated on the front of the other two. The samples with silver as the front electrode exhibited photovoltaic effects, whereas the samples with indium as the front electrode did not. This indicates that the sensitive contact is between the silver and the reoxidized rutile and not between the reduced rutile and the reoxidized rutile.

(c) Four samples were reduced together. Each sample was then reoxidized separately. The depth of the reoxidized layer was increased from sample to sample by increasing the re-oxidation temperature (see Table I). The time constant increased from  $100\ \mu\text{s}$  to  $15\ \text{msec}$  with increasing reoxidation. All samples had a spectral response peak at  $320\ \text{m}\mu$ .

TABLE I. EFFECT OF REOXIDATION ON TIME CONSTANT OF RUTILE DETECTORS

Sample	Reduction Time at 600°C (hours)	Oxidation Time (minutes)	Oxidation Temperature (°C)	d-c Resistance		Time Constant (msec)
				Reverse Bias (Ω)	Forward Bias (Ω)	
1-F	2	10	625	2600	1500	15
2-F	2	10	600	560	555	0.25
3-F	2	10	550	140	140	0.1
4-F	2	10	500	120	120	0.1

(d) Transmission measurements were made on fully oxidized, chemically deposited rutile films. The thinnest film had 40% transmission at 300 mμ. The cutoff wavelength increased with increasing thickness.

From the results of these experiments we can propose a model for the reduced-reoxidized rutile detector. First, the silver-to-reoxidized-rutile junction is sensitive. Thus, the barrier layer is formed at this junction. Photons are absorbed in or near this junction, creating hole-electron pairs. The holes and electrons diffuse to the barrier layer and result in a photovoltaic effect. The width of the barrier layer plus the diffusion length for free carriers determines the wavelength at peak spectral response. That is, peak response will occur at that wavelength for which the absorption coefficient is sufficiently high that the carriers are generated within a diffusion length of the barrier layer, but not so high that surface recombination effects reduce the responsivity. Increasing reoxidation increases the time constant by increasing the resistance of inactive bulk  $\text{TiO}_2$  in series with the active barrier layer.

The bulk of the sample which is strongly reduced acts only as a contact to the reoxidized rutile layer.

3.3.9. SPACE-CHARGE-LIMITED CURRENTS. In order to further our understanding of photoresponse and time constants in rutile, the characteristics of current flow and trapping mechanisms were studied. Only at low applied voltages do these materials obey Ohm's law; at higher voltages space-charge currents dominate the ohmic conduction. The magnitude of the space charge is given by (see Appendix B)

$$Q_{sp} = CV \text{ coulombs/cm}^2 \quad (13)$$

where  $Q_{sp}$  = space charge/cm<sup>2</sup>  
 $C$  = capacitance/cm<sup>2</sup>  
 $V$  = applied voltage

The space-charge current in trap-free material is given by

$$I = \pi \frac{\mu k}{d^3} V^2 \text{ amp/cm}^2 \quad (14)$$

where  $I$  = steady-state space-charge current

$\pi$  = constant =  $10^{-13}$

$\mu$  = mobility of carriers

$k$  = dielectric constant

$d$  = separation of capacitor plates in centimeters

In material containing traps the space-charge current is reduced by the immobilization of the current carriers in the traps. For the simplest case in which trap-state energy levels are evenly distributed throughout the forbidden gap, the following relation is obtained:

$$I = KV \exp(\beta V) \quad (15)$$

with

$$\beta = \frac{C}{n_t dekT} \quad (16)$$

where  $K$  = constant

$n_t$  = number of traps/cm<sup>3</sup>/unit energy range within the forbidden gap

$e$  = electronic charge

$k$  = Boltzmann constant

$T$  = temperature in degrees Kelvin

In materials containing traps one can observe current proportional to the square of the voltage by using pulsed application of bias. In this case the current-voltage relation is determined in a transient condition before the current carriers have a chance to be immobilized in the traps.

Since the trapping (and the releasing from traps) of space-charge-current carriers contributes to the noise of the detector, the distribution of traps in rutile (and to a lesser extent in zinc sulfide) was studied. Figure 18 is a plot of  $I/V$  vs.  $V$  for a rutile sample. Interpreting this plot on the basis of Equation 15, one finds that the trap density varies between  $10^{13}/\text{cm}^3\text{-ev}$  and  $10^{14}/\text{cm}^3\text{-ev}$ . It should be pointed out that the voltage-current data varies from sample to sample and that the slopes of these curves vary according to the past history of the sample.

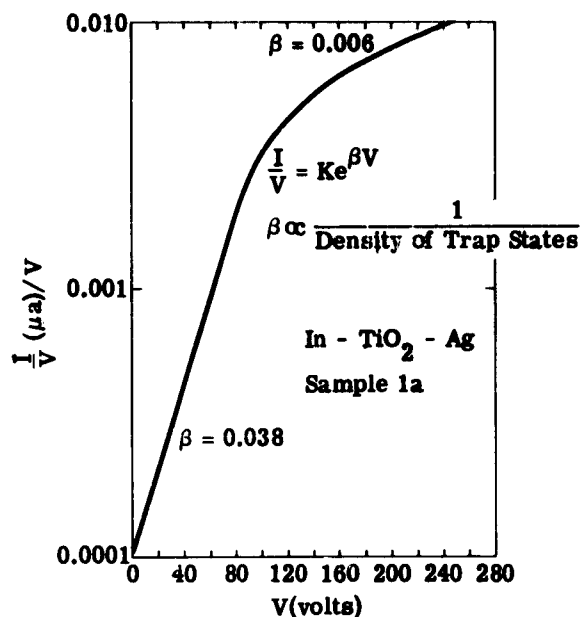


FIGURE 18. EFFECT OF TRAP STATES  
ON REDUCED CURRENT (RUTILE)

### 3.4. OTHER MATERIALS

Several other semiconductors were investigated as possible materials for ultraviolet detectors.

Magnesium oxide was obtained from Semi-Elements, Inc., in the form of a single crystal boule. Transmission measurements on a disc 1 mm thick showed an optical absorption edge at about 250  $\mu$ . Several samples were ground and polished to a thickness of 75  $\mu$ . Indium and silver electrodes were evaporated on opposite faces of a slab. This sample showed photoconductive response at wavelengths less than 260  $\mu$ , with a time constant of approximately 5 msec.

Several barium titanate single crystals in the form of thin platelets were imperfect and cleaved quite readily; thus they were hard to polish. Two samples approximately 125  $\mu$  thick were prepared. They appeared to be photosensitive, but the results were not conclusive. Transmission measurements indicated an optical cutoff at 410  $\mu$ .

A thin, nonuniform film of tin oxide was prepared by spraying a solution of tin chloride, antimony trioxide, hydrochloric acid, and water onto a glass surface held at approximately 400°C. Silver paste contacts were applied. The films were photosensitive to 365  $\mu$  radiation.

## SUMMARY AND CONCLUSIONS

Techniques have been developed for fabricating fast solid-state detectors which are sensitive in the ultraviolet spectral region. Barrier-layer devices made by the use of silver-to-rutile contacts have resulted in photovoltaic detectors with time constants of less than 100  $\mu\text{sec}$ . These detectors exhibit peak responsivity at 320  $m\mu$ , at which wavelength  $D^*$  values of  $4.5 \times 10^9 \text{ cm cps}^{1/2}/\text{watt}$  have been observed. A copper-to-zinc sulfide contact has resulted in a photovoltaic detector with time constant of 120  $\mu\text{sec}$ , but with peak spectral response occurring at 339  $m\mu$ . This detector had a  $D^*$  peak of  $9.7 \times 10^8 \text{ cm cps}^{1/2}/\text{watt}$ . It is apparent that a reduction in the resistance of the bulk semiconductor in series with the barrier layer was the primary factor in reducing the time constant from the initially observed values, which were as high as one second. With rutile the reduction in resistance was accomplished through chemical reduction of the bulk material. The bulk resistance of the zinc sulfide detector was reduced by a mechanical reduction in thickness. It is reasonable to assume that these or similar techniques could be applied to other large bandgap semiconductors.

Photoconductive response at wavelengths less than 260  $m\mu$  has been observed with magnesium oxide. Barium titanate single crystals also appear photosensitive. It appears that fast detectors sensitive at wavelengths much shorter than those mentioned above can be fabricated.

Trap states are present in both the zinc sulfide and rutile materials. However, techniques intended to empty the trap states had no effect on the time constants of even the fastest detectors. This suggests that the bulk resistance is still the time-constant limiting effect and that there is room for improvement.

The noise level of the detectors operated in the photovoltaic mode is close to that expected from thermal agitation or Johnson noise. This can be improved by cooling.

The responsivity of the detectors is the major area where improvement is necessary. The detectors are far from background-limited. A more thorough treatment of the factors involved in determining responsivity (and time constant) is indicated.

## Appendix A

### EQUIVALENT-CIRCUIT ANALYSIS

To determine whether the capacitance and high resistance inherent in barrier layer detectors made from relatively thick samples of high-resistivity material could influence the time constant of the detectors, we made the following circuit analysis. The equivalent circuit (Diagram 1) used to represent the junction detector was that discussed by Walter [10]

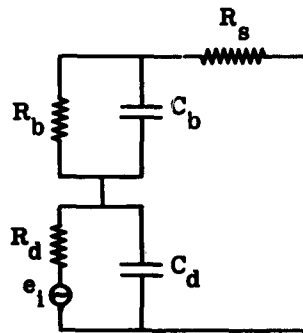


DIAGRAM 1

where  $C_d$  = capacity of depletion layer  
 $R_d$  = resistance of depletion layer  
 $C_b$  = capacity of bulk region  
 $R_b$  = resistance of bulk region  
 $R_s$  = any additional series resistance

If chopped ultraviolet radiation is incident on the detector, a voltage generator,  $e_i$ , can be inserted in the circuit as shown. Since  $R_s$  is mainly contact resistance and is small compared to  $R_b$  and  $R_d$ , it will be ignored.

The overall equivalent circuit (Diagram 2) then becomes

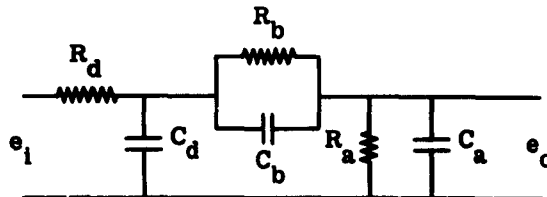


DIAGRAM 2

where  $e_o$  = output voltage

$C_a$  = input capacity of amplifier

$R_a$  = input resistance of amplifier

In a simplified form (Diagram 3)

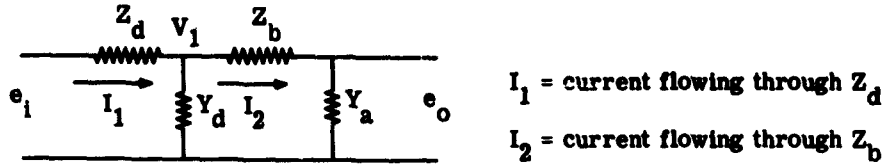


DIAGRAM 3

$$\text{where } Y_a = SC_a + \frac{1}{R_a}$$

$$Z_b = \frac{R_b}{SR_b C_b + 1}$$

$$Y_d = SC_d$$

$$Z_d = R_d$$

and where  $S$  =  $S$  of Laplace transform notation [11].

The transfer function  $e_o/e_{i(s)}$  will now be developed. Starting from  $e_o$  and working to the left, we have the following relationships:

$$I_2 = e_o Y_a$$

$$V_1 = I_2 Z_b + e_o = e_o Y_a Z_b + e_o$$

$$I_1 = I_2 + V_1 Y_d = e_o Y_a + e_o Y_a Z_b Y_d + e_o Y_d$$

$$e_i = I_1 Z_d + V_1 = e_o Y_a Z_d + e_o Y_a Z_b Y_d Z_d + e_o Y_d Z_d + e_o Y_a Z_b + e_o$$

$$\therefore \frac{e_o}{e_i} = \frac{1}{(Y_a Z_d + Y_a Z_b Y_d Z_d + Y_d Z_d + Y_a Z_b + 1)}$$

Substituting for Y's and Z's, we have

$$\frac{e_o}{e_i} = \frac{1}{\left( \frac{SR_d C_a + R_d}{R_a} \right) + \left[ \left( \frac{SR_a C_a + 1}{R_a} \right) \left( \frac{R_b}{SR_b C_b + 1} \right) (SR_d C_d) \right] + (SR_d C_d) + \left[ \left( \frac{SR_a C_a + 1}{SR_b C_b + 1} \right) \cdot \frac{R_b}{R_a} \right] + 1}$$

$$= \frac{SR_b C_b + 1}{s^2 R_d C_a R_b C_b + s \left( R_d C_a + R_b C_b \frac{R_d}{R_a} \right) + \frac{R_d}{R_a} + s^2 R_d C_d R_b C_a + SR_d C_d \frac{R_b}{R_a} + s^2 R_d C_d R_b C_b + SR_d C_d + SR_b C_a + \frac{R_b}{R_a} + SC_b R_b + 1}$$

$$\therefore \frac{e_o}{e_i} = \frac{SK_1 + 1}{s^2 K_2 + SK_3 + K_4}$$

where  $K_1 = C_b R_b$

$$K_2 = R_d C_a R_b C_b + R_d C_d R_b C_a + R_d C_d R_b C_b$$

$$K_3 = R_d C_a + R_b C_b \frac{R_d}{R_a} + R_d C_d \frac{R_b}{R_a} + R_d C_d + R_b C_a + R_b C_b$$

$$K_4 = \frac{R_d}{R_a} + \frac{R_b}{R_a} + 1 = \frac{R_d + R_b + R_a}{R_a}$$

$$\frac{e_o}{e_i} = \frac{SK_1}{s^2 K_2 + SK_3 + K_4} + \frac{1}{s^2 K_2 + SK_3 + K_4} = \frac{SK_1/K_2}{(s + \beta_1)(s + \beta_2)} + \frac{1/K_2}{(s + \beta_1)(s + \beta_2)}$$

$$\text{where } \beta_1 = \frac{K_3}{2K_2} + \frac{\sqrt{K_3^2 - 4K_2 K_4}}{2K_2}$$

$$\beta_2 = \frac{K_3}{2K_2} - \frac{\sqrt{K_3^2 - 4K_2 K_4}}{2K_2}$$

For a step input voltage, as would be generated by a chopped ultraviolet source

$$e_i(s) = V_o/s$$

For this analysis we will assume that  $V_o = 1$ . Therefore

$$e_o = \frac{1}{K_2} \left[ \frac{K_1}{(s + \beta_1)(s + \beta_2)} + \frac{1}{s(s + \beta_1)(s + \beta_2)} \right]$$

$$= \frac{1}{K_2} \left[ K_1 \left( \frac{A}{s + \beta_1} + \frac{B}{s + \beta_2} \right) + \frac{C}{s} + \frac{D}{s + \beta_1} + \frac{E}{s + \beta_2} \right]$$

$$\text{where } A = -\frac{1}{\beta_1 - \beta_2}$$

$$B = \frac{1}{\beta_1 - \beta_2}$$

$$C = \frac{1}{\beta_1 \beta_2}$$

$$D = \frac{1}{\beta_1(\beta_1 - \beta_2)}$$

$$E = -\frac{1}{\beta_2(\beta_1 - \beta_2)}$$

$$\therefore e_o(s) = \frac{1}{K_2} \left[ \frac{K_1}{\beta_1 - \beta_2} \left( \frac{1}{s + \beta_2} - \frac{1}{s + \beta_1} \right) + \frac{1}{\beta_1 \beta_2 s} + \frac{1}{\beta_1(\beta_1 - \beta_2)(s + \beta_1)} - \frac{1}{\beta_2(\beta_1 - \beta_2)(s + \beta_2)} \right]$$

$$= \frac{1}{K_2} \left\{ \frac{1}{\beta_1 \beta_2 s} + \frac{1}{\beta_1 - \beta_2} \left[ \left( K_1 - \frac{1}{\beta_2} \right) \cdot \frac{1}{s + \beta_2} - \left( K_1 - \frac{1}{\beta_1} \right) \cdot \frac{1}{s + \beta_1} \right] \right\}$$

$$\therefore e_o(t) = \frac{1}{K_2} \left\{ \frac{1}{\beta_1 \beta_2} + \frac{1}{\beta_1 - \beta_2} \left[ \left( K_1 - \frac{1}{\beta_2} \right) e^{-\beta_2 t} - \left( K_1 - \frac{1}{\beta_1} \right) e^{-\beta_1 t} \right] \right\}$$

This indicates that the response of the circuit will have two time constants,  $1/\beta_1$  and  $1/\beta_2$ .

Substituting representative values for the 25 $\mu$ -thick ZnS detector, one finds

$$R_d \cong 5 \times 10^8 \Omega$$

$$C_d \cong 10^{-10} \text{ f} \cong \text{detector capacity}$$

$$R_b \cong 5 \times 10^9 \cong \text{static d-c detector resistance}$$

$$C_b \cong 5 \times 10^{-11} \text{ f}$$

$$R_a \cong 5 \times 10^8 \Omega \cong \text{input resistor of cathode follower}$$

$$C_a \cong 7 \times 10^{-12} \text{ f} \cong \text{inter-electrode capacity of cathode follower tube}$$

$$K_1 \approx 2.5 \times 10^{-1}$$

$$K_2 \approx 0.0875 \times 10^{-2} + 0.175 \times 10^{-2} + 1.25 \times 10^{-2} \approx 1.5 \times 10^{-2}$$

$$K_3 \approx 0.0035 + 0.25 + 0.50 + 0.05 + 0.035 + 0.25 \\ = 1.1$$

$$K_4 \approx 12$$

$$\beta_1 \approx \frac{K_3}{2K_2} + \frac{\sqrt{K_3^2 - 4K_2K_4}}{2K_2}$$

$$\approx 37 + 23$$

$$\approx 60$$

$$\beta_2 \approx 37 - 23$$

$$\approx 14$$

$$\therefore \tau_1 = 17 \text{ msec}$$

$$\tau_2 = 71 \text{ msec}$$

$$\therefore e_o(t) = 0.08 + 0.26 \exp(-14t) - 0.34 \exp(-60t)$$

These values agree reasonably well with those observed for the ZnS detectors (see Section 3.2). Figure 19 is a plot of the output voltage as a function of time  $[e_o(t)]$  to be expected under the conditions given above. The similarity between the response and that shown in Figure 19 is evident.

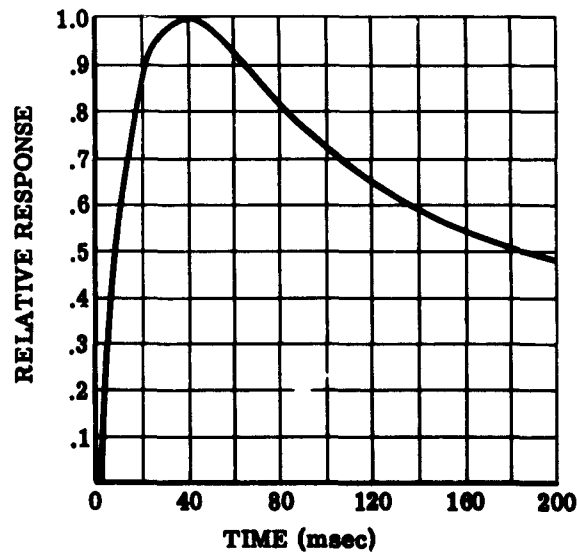


FIGURE 19. RESPONSE OF EQUIVALENT CIRCUIT TO STEP INPUT

## Appendix B

### SPACE-CHARGE-LIMITED CURRENTS

Let two plane parallel electrodes separated by a dielectric have a capacitance  $C/\text{cm}^2$ . The magnitude of the space charge which results from an applied voltage,  $V$ , is given by the familiar relation:

$$Q_{\text{sp}} = CV \text{ coulombs/cm}^2 \quad (17)$$

There will in general be a current,  $I$ , flowing from one electrode to the other, given by:

$$I = \frac{Q}{T} = \frac{CV}{t} \text{ amp/cm}^2 \quad (18)$$

where  $t$  is the time required for a unit of charge to drift from electrode to the other.

The current,  $I$ , is known as the space-charge-limited current. SCLC is often small compared to ohmic currents. However, in near insulators it can be dominant.

In order to observe SCLC it is necessary that at least one electrode be capable of injecting carriers into the dielectric. Rose has shown that SCLC can be a valuable tool for measuring imperfections in insulating crystals [12]. He derived current-voltage relations which can be used to determine the energy distribution of traps in an insulator. They are reviewed briefly below.

The  $C/\text{cm}^2$  of a parallel plate capacitor is given by

$$C = \frac{k}{4\pi d} \times 10^{-12} \text{ f} \quad (19)$$

where  $k$  = dielectric constant of the insulator between electrodes

$d$  = distance between electrodes in centimeters

The transit time  $t$  is

$$t = \frac{d^2}{V\mu} \quad (20)$$

where  $\mu$  is the drift mobility.

Combining Equations 18, 19, and 20 gives the SCLC for the trap free case

$$I = \frac{\mu k}{d^3} 10^{-13} V^2 \quad (21)$$

For an insulator with traps, one replaces the drift mobility,  $\mu$ , with the drift mobility for free carriers,  $\mu_0$ , times the fraction of the total space charge that is free,  $\theta$ .

$$I = \frac{\mu_0 \theta k}{d^3} 10^{-13} V^2 \quad (22)$$

If the traps are close enough to the conduction band to be in thermal equilibrium with the electrons in that band,  $\theta$  will not be a function of voltage. Equation 22 will then be the correct current-voltage relation for an insulator with shallow traps.

If one assumes a uniform distribution of traps below the conduction band,  $\theta$  is given by

$$\theta = \frac{e n_c d}{VC} \exp(\beta V) \quad (23)$$

where  $e$  = electronic charge

$n_c$  = free carrier density

$$\beta = \frac{C}{n_t d e k T}$$

$n_t$  = number of traps/cm<sup>3</sup>/unit energy range within the forbidden gap

$k$  = Boltzmann constant

$T$  = absolute temperature

From Equations 22 and 23 we obtain

$$I = KV \exp(\beta V) \quad (24)$$

where  $K$  is independent of voltage for a uniform distribution of traps.

If the trap distribution varies exponentially with energy,  $E$ , measured from the bottom of the conduction band

$$n_t = A \exp(-E/kT_c) \quad (25)$$

where  $T_c$  is some characteristic temperature; then, Rose has shown, the SCLC is

$$I = BV^{\frac{T_c}{T} + 1} \quad (26)$$

## REFERENCES

1. D. A. Cusano, "Radiation-Controlled Electroluminescence and Light Amplification in Phosphor Films" Phys. Rev., 1955, Vol. 98, p. 546.
2. R. G. Breckenridge and W. R. Hosler, "Titanium Dioxide Rectifiers," J. Res. Nat. Bur. Std., 1952, Vol. 49, p. 65.
3. R. A. Smith, Semiconductors, Cambridge Press, London, 1961.
4. D. A. Wright, Semi-Conductors, Methuen and Co., Ltd., London, 1950.
5. R. H. Bube, Photoconductivity of Solids, Wiley and Sons, Inc., New York, 1960.
6. T. S. Moss, Optical Properties of Semi-Conductors, Academic Press, Inc., New York, 1959.
7. F. A. Grant, "Properties of Rutile (Titanium Dioxide)," Rev. Mod. Phys., 1959, Vol. 31, p. 646.
8. D. C. Cronmeyer, "Electrical and Optical Properties of Rutile Single Crystals," Phys. Rev., 1952, Vol. 87, p. 876.
9. R. G. Breckenridge and W. R. Hosler, "Electrical Properties of Titanium Dioxide Semiconductors," Phys. Rev., 1953, Vol. 91, p. 793.
10. F. J. Walter, "Discussion of Pulse Rise Times and Equivalent Circuits," Semiconductor Nuclear Particle Detectors, National Academy of Sciences—National Research Council, Washington, D. C., Publication 871, 1960, p. 238.
11. R. V. Churchill, Modern Operational Mathematics in Engineering, McGraw-Hill Book Company, Inc., New York, 1944.
12. A. Rose, "Space-Charge-Limited Currents in Solids," Phys. Rev., 1955, Vol. 97, p. 1538.

<p>Aeronautical Systems Division, Dir/Avionics, Electronic Technology Lab, Wright-Patterson AFB, Ohio.</p> <p>Rpt Nr ASD-TDR-62-978, DEVELOPMENT OF A FAST SOLID-STATE ULTRAVIOLET PHOTODETECTOR. Final report, Mar 63, 33p. incl illus., tables, 12 refs.</p> <p>Unclassified report</p> <p>The objective of this work was to develop a fast solid-state ultraviolet detector. Efforts were concentrated on photovoltaic devices using metal semiconductor barrier layers. Peak detectivities of <math>10^9</math> cm cps<math>^{1/2}</math>/watt</p> <p>(over)</p>	<ol style="list-style-type: none"> <li>1. Ultraviolet detectors</li> <li>2. Fast solid-state detectors</li> <li>3. Optical detectors</li> <li>4. Barrier-layer detectors</li> <li>5. Photoelectric cells</li> </ol> <ol style="list-style-type: none"> <li>I. AFSC Project 4460, Task 446004</li> <li>II. Contract AF 33(616)-8410</li> <li>III. The University of Michigan, Ann Arbor, Michigan</li> </ol>	<p>Aeronautical Systems Division, Dir/Avionics, Electronic Technology Lab, Wright-Patterson AFB, Ohio.</p> <p>Rpt Nr ASD-TDR-62-978, DEVELOPMENT OF A FAST SOLID-STATE ULTRAVIOLET PHOTODETECTOR. Final report, Mar 63, 33p. incl illus., tables, 12 refs.</p> <p>Unclassified report</p> <p>The objective of this work was to develop a fast solid-state ultraviolet detector. Efforts were concentrated on photovoltaic devices using metal semiconductor barrier layers. Peak detectivities of <math>10^9</math> cm cps<math>^{1/2}</math>/watt</p> <p>(over)</p>	<ol style="list-style-type: none"> <li>1. Ultraviolet detectors</li> <li>2. Fast solid-state detectors</li> <li>3. Optical detectors</li> <li>4. Barrier-layer detectors</li> <li>5. Photoelectric cells</li> </ol> <ol style="list-style-type: none"> <li>I. AFSC Project 4460, Task 446004</li> <li>II. Contract AF 33(616)-8410</li> <li>III. The University of Michigan, Ann Arbor, Michigan</li> </ol>
<p>and time constants of less than 120 <math>\mu</math>sec were achieved with both ZnS (<math>\lambda</math> peak = 339 m<math>\mu</math>) and TiO<math>_2</math> (<math>\lambda</math> peak = 320 m<math>\mu</math>). MgO was found to be photoconductive when exposed to radiation of wavelength less than 260 m<math>\mu</math>. Trapping states in TiO<math>_2</math> were investigated by means of the method of space-charge-limited currents.</p> <p>(over)</p>	<ol style="list-style-type: none"> <li>IV. Douglas E. Brown, Richard C. Keezer, Joseph Mudar</li> <li>V. 4611-13-F</li> <li>VI. Aval fr OTS</li> <li>VII. In ASTIA collection</li> </ol>	<p>and time constants of less than 120 <math>\mu</math>sec were achieved with both ZnS (<math>\lambda</math> peak = 339 m<math>\mu</math>) and TiO<math>_2</math> (<math>\lambda</math> peak = 320 m<math>\mu</math>). MgO was found to be photoconductive when exposed to radiation of wavelength less than 260 m<math>\mu</math>. Trapping states in TiO<math>_2</math> were investigated by means of the method of space-charge-limited currents.</p> <p>(over)</p>	<ol style="list-style-type: none"> <li>IV. Douglas E. Brown, Richard C. Keezer, Joseph Mudar</li> <li>V. 4611-13-F</li> <li>VI. Aval fr OTS</li> <li>VII. In ASTIA collection</li> </ol>